

Supporting Information Available

In situ diffusion growth of Fe₂(MoO₄)₃ nanocrystals on the surface of α-MoO₃ nanorods with significantly enhanced ethanol sensing properties

Yujin Chen, *^a Fana Meng, ^a Chao Ma, ^b Zhiwei Yang, ^{b,c} Chunling Zhu, ^d Qiuyun Ouyang, ^a Peng Gao, *^d Jianqi Li, ^b and Chunwen Sun *^{b,c}

^a College of Science, Harbin Engineering University, Harbin, 150001, China

^b Beijing National Laboratory for Condensed Matter Physics, Institute of Physics, Chinese Academy of Sciences, Beijing, 100190, China

^c Key Laboratory for Renewable Energy, Chinese Academy of Sciences, Beijing, 100190, China

^d College of Material Science and Chemical Engineering, Harbin Engineering University, Harbin, 150001, China

E-mail: chenyujin@hrbeu.edu.cn; csun@iphy.ac.cn and gaopeng@hrbeu.edu.cn

SI-1 SEM image of α-MoO₃ nanorods

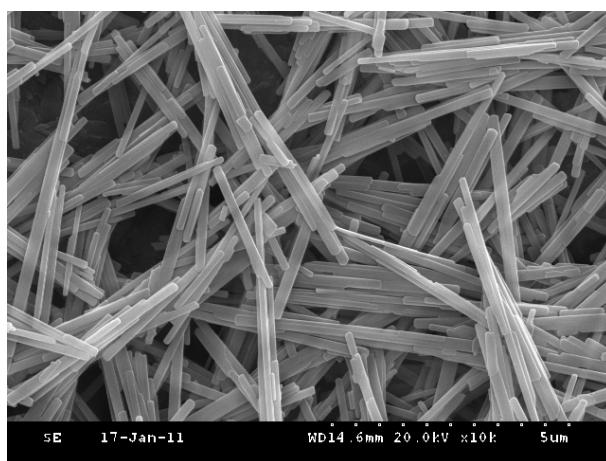


Figure S1 A typical SEM image of the pristine α-MoO₃ nanorods

SI-2 STEM images and the electron energy loss spectroscopy analysis of Fe(OH)₃@ α -MoO₃ nanorods

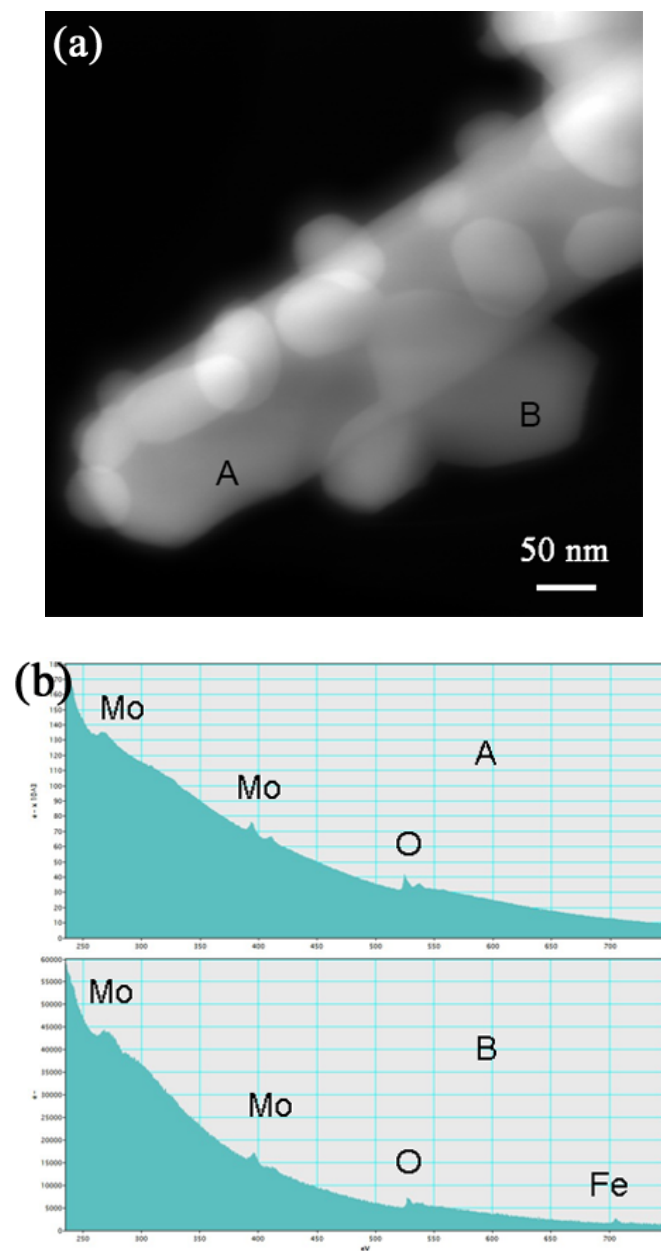


Figure S2 (a) STEM image of the $\text{Fe}_2(\text{MoO}_4)_3@\text{MoO}_3$ nanorod, and (b) the electron energy loss spectroscopy analysis taken at A and B areas in (a).

SI-3 SEM images of Fe(OH)₃@α-MoO₃ nanorods



Figure S3 A typical SEM images of Fe(OH)₃@α-MoO₃ nanorods.

SI-4 XRD pattern of Fe(OH)₃@α-MoO₃ nanorods

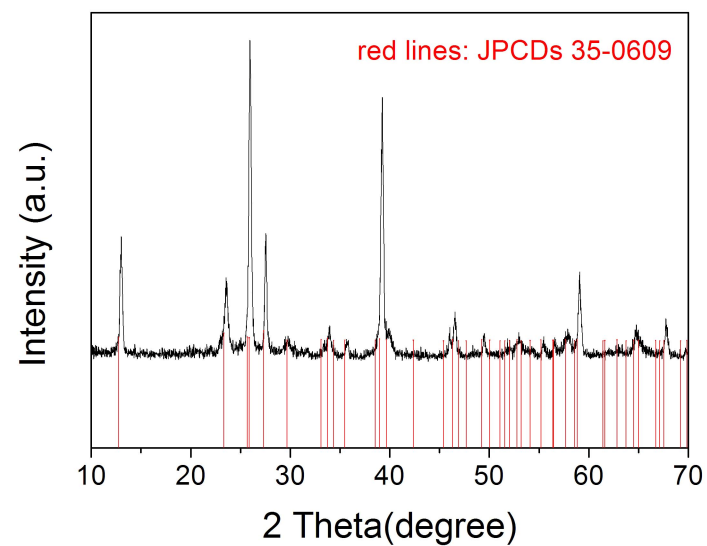


Figure S4 XRD pattern of the as-prepared Fe(OH)₃@α-MoO₃ nanorods

SI-5 TEM image of the sample obtained at 500°C for 1h

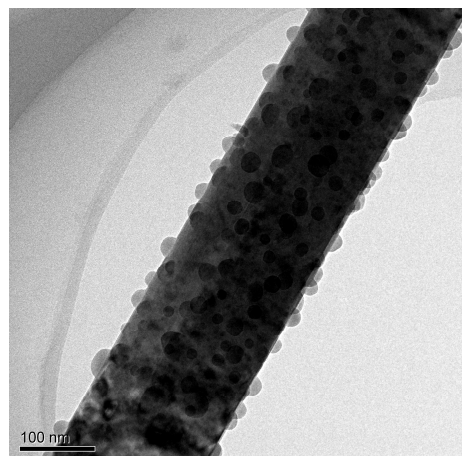


Figure S5 TEM image of the sample obtained at 500°C for 1 h.

SI-6 TEM image of the sample obtained at 500°C for 2 h

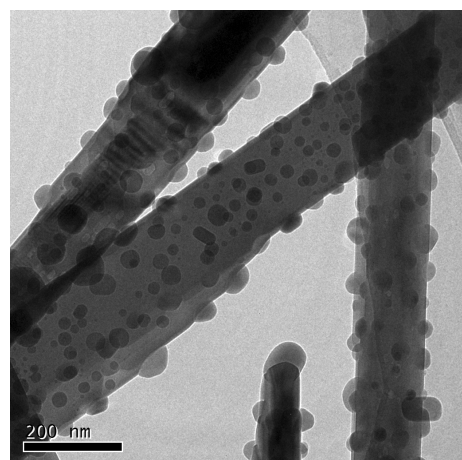


Figure S6 TEM image of the sample obtained at 500°C for 2 h.

SI-7 TEM image of the sample obtained at 500 °C for 3 h

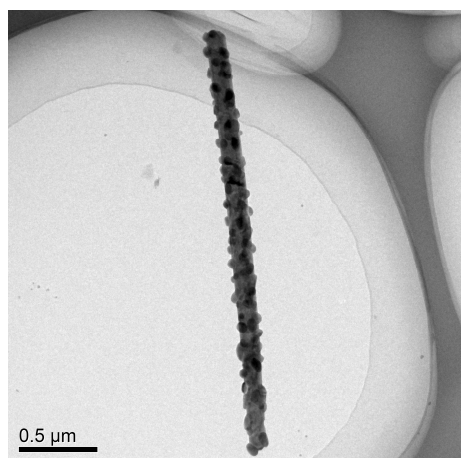


Figure S7 TEM image of the sample obtained at 500 °C for 3 h.

SI-8 Preparation of Fe₂(MoO₄)₃ nanocrystals and structural characterization

20 mL of 0.2 mol L⁻¹ Fe(NO₃)₃ aqueous solution was added into 50 mL of 0.12 mol L⁻¹ (NH₄)₆Mo₇O₂₄ aqueous solution under stirring. The mixture was stirred for 10 min. The precipitate was dried and then thermally treated at 500 °C for 4 h.

Fig. S9 shows the XRD pattern of the final product, in which blue lines denote the locations of the standard diffraction peaks of the monclinic Fe₂(MoO₄)₃ (JCPDS, 83-1701, cell parameters: $a = 15.70\text{ \AA}$, $b = 9.231\text{ \AA}$, $c = 18.20\text{ \AA}$, $\beta = 125.2^\circ$). Compared with the standard data, all peaks, marked by Miller indices, can be indexed to monclinic Fe₂(MoO₄)₃. This reveals that the product mainly consists of crystallized Fe₂(MoO₄)₃.

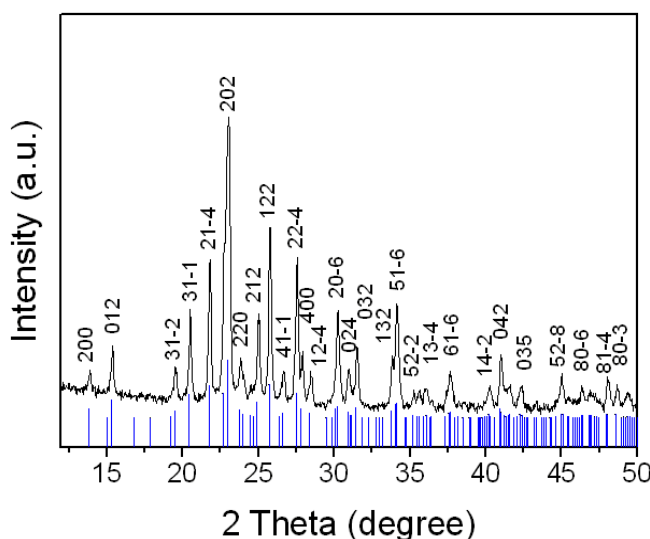


Figure S8 XRD pattern of crystalline $\text{Fe}_2(\text{MoO}_4)_3$ particles.

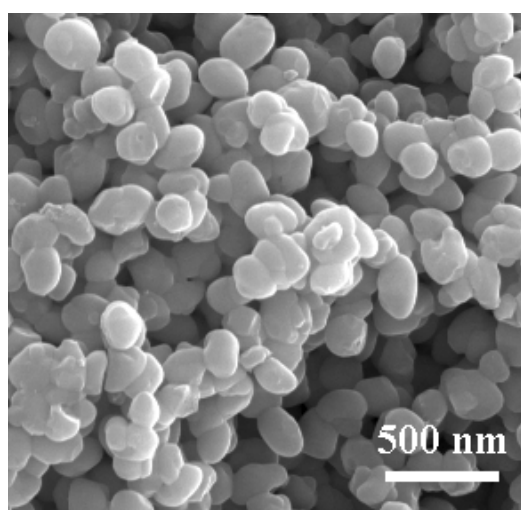


Figure S9 SEM image of crystalline $\text{Fe}_2(\text{MoO}_4)_3$ nanoparticles.

Fig. S9 shows a typical SEM image of crystallized $\text{Fe}_2(\text{MoO}_4)_3$ nanoparticles. It can be seen that an average diameter of $\text{Fe}_2(\text{MoO}_4)_3$ nanoparticles is about 200 nm.

SI-9 Sensor responses of $\text{Fe}_2(\text{MoO}_4)_3@\alpha\text{-MoO}_3$ nanorods and $\text{Fe}_2(\text{MoO}_4)_3$ nanoparticles to 10 ppm ethanol

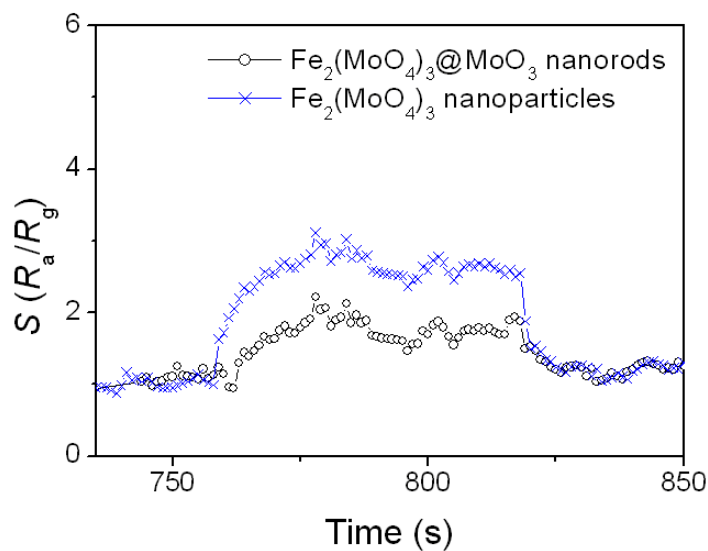


Fig. S10 Sensor responses of $\text{Fe}_2(\text{MoO}_4)_3@\alpha\text{-MoO}_3$ nanorods and $\text{Fe}_2(\text{MoO}_4)_3$ nanoparticles to 10 ppm ethanol at 220 °C.

SI-10 Stability of $\text{Fe}_2(\text{MoO}_4)_3@\alpha\text{-MoO}_3$ nanorods to 100 ppm ethanol

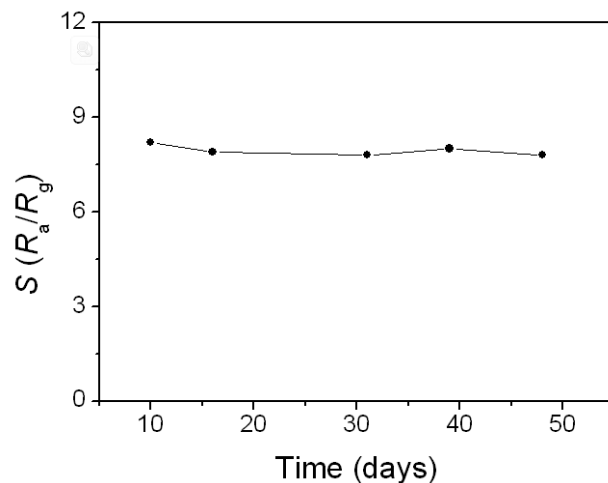


Fig. S11 Long-term stability of the $\text{Fe}_2(\text{MoO}_4)_3@\alpha\text{-MoO}_3$ nanorods to 100 ppm ethanol at 220 °C.

SI-11 EDS patterns of the obtained $\text{Fe}_2(\text{MoO}_4)_3@\alpha\text{-MoO}_3$ nanorods by adding different amounts of $\text{Fe}(\text{NO}_3)_3 \cdot 9\text{H}_2\text{O}$

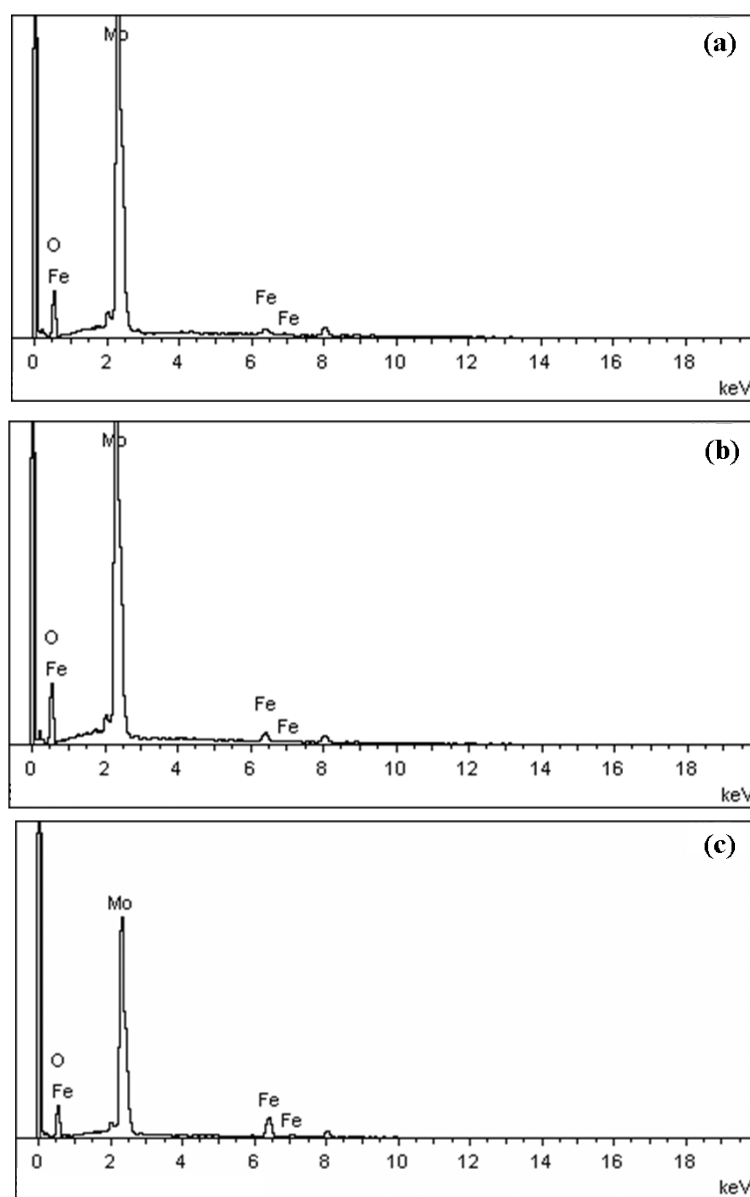


Fig. S12 EDS patterns of the obtained $\text{Fe}_2(\text{MoO}_4)_3@\alpha\text{-MoO}_3$ nanorods by adding different amounts of $\text{Fe}(\text{NO}_3)_3 \cdot 9\text{H}_2\text{O}$: (a) 0.1 g of $\text{Fe}(\text{NO}_3)_3 \cdot 9\text{H}_2\text{O}$, (b) 0.3 g of $\text{Fe}(\text{NO}_3)_3 \cdot 9\text{H}_2\text{O}$ and (c) 0.6 g of $\text{Fe}(\text{NO}_3)_3 \cdot 9\text{H}_2\text{O}$.

Fig. S12 shows EDS patterns of the $\text{Fe}_2(\text{MoO}_4)_3@\alpha\text{-MoO}_3$ nanorods obtained by adding different amount of $\text{Fe}(\text{NO}_3)_3 \cdot 9\text{H}_2\text{O}$ into the reaction solution. The molar ratios of Mo to Fe for the samples obtained by adding 0.1 g, 0.3g, 0.6g of

$\text{Fe}(\text{NO}_3)_3 \cdot 9\text{H}_2\text{O}$, are 17.7:1, 7.5:1 and 4:1, respectively. It indicates that the content of $\text{Fe}_2(\text{MoO}_4)_3$ nanocrystals in the nanocomposites is increased with increasing $\text{Fe}(\text{NO}_3)_3 \cdot 9\text{H}_2\text{O}$ amount.

SI-12 Selectivity of the $\text{Fe}_2(\text{MoO}_4)_3 @ \alpha\text{-MoO}_3$ nanorods to different gases

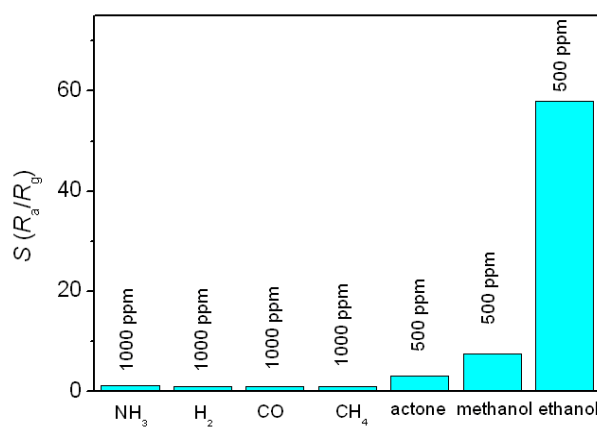


Fig. S 13 The sensitivity of the $\text{Fe}_2(\text{MoO}_4)_3 @ \alpha\text{-MoO}_3$ nanorods to other gases at 220 °C.

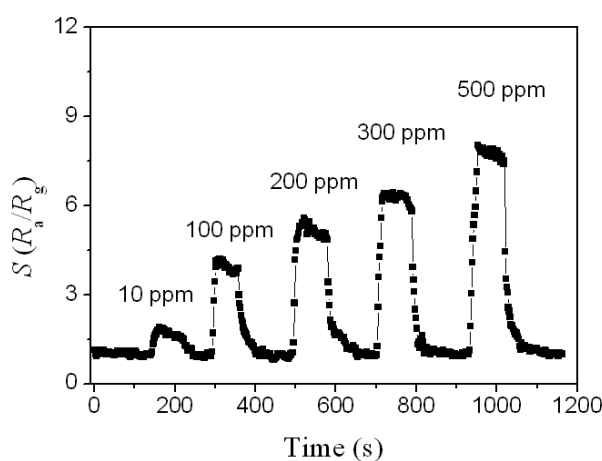


Fig. S 14 Time-dependent response of the $\text{Fe}_2(\text{MoO}_4)_3 @ \alpha\text{-MoO}_3$ nanorods to methanol with different concentrations at 220 °C.